Applied Catalysis B: Environmental 115–116 (2012) 276–284

Contents lists available at SciVerse ScienceDirect

Applied Catalysis B: Environmental

journal homepage: www.elsevier.com/locate/apcatb

Photocatalytic degradation of Rhodamine 6G on mesoporous titania films: Combined effect of texture and dye aggregation forms

M.N. Ghazzal[a,*], H. Kebaili[b], M. Joseph[a], D.P. Debecker[a], P. Eloy[a], J. De Coninck[b], E.M. Gaigneaux[a]

[a] Institute of Condensed Matter and Nanoscience – Molecules, Solids and Reactivity (IMCN/MOST), Université catholique de Louvain, Croix du Sud 2/17, 1348 Louvain-La-Neuve, Belgium

[b] Université de Mons – UMONS, Laboratoire de physique des surfaces et interfaces, 20 Place du Parc, 7000 Mons, Belgium

ARTICLE INFO

Article history:
Received 11 September 2011
Received in revised form 2 December 2011
Accepted 9 December 2011
Available online 17 December 2011

Keywords:
Mesoporous film
TiO_2
Photocatalysis
Dye aggregation
Rhodamine 6G

ABSTRACT

Titania films with different textural properties have been synthesized using the sol–gel spin-coating process. Titania sols were prepared with and without non ionic template agents, Pluronic® P123 and Brij56®, in order to evaluate the effect of the surface developed by the films on their photocatalytic activity. The morphology, surface composition, open porosity and pore size distribution of these films were investigated by transmission electronic microscopy, X-ray photoelectron spectroscopy and atmospheric ellipsometric porosimetry. The optical properties of the titania films were evaluated by UV–vis transmittance spectroscopy. The porosity released after burning the template at 400 °C reduces the refractive index of the coatings and the transmittance in the visible range becomes equal for naked and coated soda lime glasses. In parallel, the photocatalytic activity of the non porous and porous titania films was evaluated by following the photodegradation kinetics of Rhodamine 6G dye. Results show that the increase of the available active surface of the titania films affects the photocatalytic activity. However, this feature was not the only parameter responsible for the improvement of the photocatalytic efficiency. The aggregation form of the Rhodamine 6G dye was also related to titania film texture. This proved to have a marked impact on the photocatalytic performances.

1. Introduction

Titanium dioxide has been the object of a strong attention as a photoactive semiconductor needing a low-energy UV excitation. Particularly, the oxidative power of the photogenerated carriers observed on TiO_2 surface and its tunable superficial hydrophobic/hydrophilic made TiO_2 one of the most attractive photocatalytic materials [1–4]. The possibility to master these two properties fostered to the emergence of a new generation of glass named self-cleaning glass (SCG, hereafter). The latter are made of glass-supported TiO_2 films.

As widely known, the photocatalytic activity has been related to intrinsic parameters of TiO_2 such as structure, specific surface area, recombination center, surface hydroxyls, crystallinity, etc. [5,6] and extrinsic parameters such as pollutant concentration, pollutant nature, pH, presence of inorganic salts, etc. [7,8]. Many studies reported the beneficial effect of the specific surface area on the photocatalytic performance of titania films. Keeping in mind that the coating weight must remain below a few pg/cm^2, this can be achieved by introducing pores in the film. Thus organic additives are classically introduced during film preparation and then removed to create or release pores. Guo et al. [9] reported that photocatalytic activity of sol–gel titania films can be improved by introducing increasing amounts of polyethylene glycol (PEG, hereafter) in the sol–gel preparation. More recently, Arconada et al. [10] compared the photocatalytic activity of dense titania films (among others) with a PEG induced porosity in the degradation of trichloroethylene in air. The authors attribute the higher activity of the latter films to the larger number of accessible reactive sites. Sakatani et al. [11] studied the effect of the calcination temperature on the photocatalytic performance of mesoporous TiO_2 films by following the bleaching of methylene blue dye (MB). The aggregation behavior of MB (i.e. formation of dimers, oligomers or persistence of monomers) on titania films surface was recently shown to be related to its concentration, with an impact on the photocatalytic performance [12]. Mills et al. [13] revealed that the photocatalytic degradation of adsorbed MB on mesoporous titanium film involves several processes and intermediate species such as J-aggregated dimer forms. However, neither the pollutant's aggregation form at the surface of the porous films nor the increase of hydroxyl number induced by the addition of the PEG in the sol–gel process [14] were taken into account in published studies. The change of the surface texture through the introduction of the porosity into the titania films modifies the dye adsorption behavior

* Corresponding author. Tel.: +32 10473660.
E-mail address: mohamed.ghazzal@uclouvain.be (M.N. Ghazzal).

0926-3373/$ – see front matter © 2011 Elsevier B.V. All rights reserved.
doi:10.1016/j.apcatb.2011.12.016

Table 1
Composition of film precursor solutions.

Samples	Precursor		Composition (mol/mol metal)				Aging temperature		
	Alkoxyde	n (M)	Solvent		H_2O	HCl	Template	n (T)/n (Ti)	
TiO_2	$Ti(OEt)_4$	0.012	1-butanol	9	–	2	–	–	25 °C
TiB	$Ti(OEt)_4$	0.012	1-butanol	9	–	2	Brij56	0.05	25 °C
TiP	$Ti(OEt)_4$	0.012	1-butanol	18	–	4	P123	0.013	25 °C

n (T)/n (Ti): molecular ratio between the template and the titanium precursor.

at the photocatalyst surface and probably influences its aggregation form.

This study follows the work proposed by Mills et al. [13] on nanoparticle titania films stained by different dyes under variable alkaline conditions and acidic conditions. Apart from the latter report, the literature on the photocatalytic destruction of adsorbed dyes in air–solid systems is scarce [13]. There are only a few reports focused on dry, dye-photocatalyst films, despite their importance as a useful test for evaluating the photocatalytic activity of self-cleaning glass [8,15,16]. Thus the present paper turns out to be the study of dry dye-photocatalyst in the actual conditions of photocatalysis. We aim at pointing out the dependence of the degradation kinetics with (i) the dye aggregation form and with (ii) the surface morphology of the films. In this way, the photocatalyst performance would not be overestimated or misleading.

The most common method to depositing dye on titania film is dip-coating [16]. Mills et al. [13] proposed an alternative method of depositing of cationic and anionic dyes on the photocatalyst surface by modifying the charge of the titania surface, which is well known to be pH dependent. Herein, we proposed to use a spin-coating as a simple, inexpensive and obvious route to depositing Rh6G on titania surfaces. This method could help to understand the adsorption behavior of Rh6G at the titanium film surface and then the kinetics of "dry dye-photocatalyst" interaction in photocatalysis. To the best of our knowledge, the aggregation form of the Rh6G deposited via spin-coating on titania films with variable surface textures, has not yet been discussed in terms of impact on the photocatalytic efficiency of the films.

In this study, different surface morphologies of inorganic titania films were prepared using one pot sol–gel method by adding or not a template agent. Rh6G is deposited at the films surfaces by means spin-coating. UV–vis absorption spectroscopy is used to characterize the aggregation forms of the dye on the film surfaces and to follow its degradation under UV-irradiation versus time. The ratio of different aggregation form is determined and correlated to the texture of the films. Moreover, the aggregation behavior of the Rh6G dye and the photocatalytic activity for different surfaces of titania films has been compared. The photocatalytic performances are elucidated on the basis of the combination of available surface area and the aggregation behavior.

2. Experimental

2.1. Material reagent

All reagents used in this work were of analytical grade and were used without any further purification: titanium(IV) tetraethoxide ($Ti(OC_2H_5)_4$, 95% Aldrich); ethanol absolute grade; 1-butanol (BuOH) (>99.4%, Alfa Aesar); hydrochloride acid (Aldrich, 37%). As structuring agent, also call hereafter template, we use a triblock copolymer, precisely polyethylene glycol hexadecyl ether (denoted Brij 56, $C_{16}H_{33}(OCH_2CH_2)_nOH$, $n \sim 10$, Aldrich) or Pluronic P123 ($M_n \sim 5800$, denoted: $EO_{20}PO_{70}EO_{20}$, Aldrich). Soda lime glass slides and indium tin oxide coated glass slides (ITO) were purchased from Aldrich.

2.2. Titania thin films synthesis

Mesoporous nanostructured TiO_2 films were prepared following a variation of a procedure reported elsewhere [17,18]. During the hydrolysis of the titanium alkoxides, highly acidic conditions were required to prevent an immediate precipitation of TiO_2. Specifically, an adequate amount of titanium (IV) tetraethoxide (TEOT) was dissolved in concentrated hydrochloric acid (37%) at room temperature. After vigorous stirring during 20 min, the hybrid solution was obtained by the addition of dissolved template into 1-butanol. The final molar ratio of the solution was 1 TEOT:2–4 HCl:9 1-butanol:x template. Table 1 summarizes the nature and the specific amounts of template used for each layer. The solutions were subsequently aged under magnetic stirring at room temperature for 3 h before the films were spin coated onto soda lime glass (SLG hereafter) or ITO-coated glass slides. ITO-coated glasses were used for ellipsometric measurements. In parallel, the mesoporous TiO_2 powder for XRD analysis was prepared following the same procedure described for the films. Briefly, the solvent was evaporated at ambient temperature and the gel formed was dried in air at room temperature for 12 h, and finally dried successively for: 6 h at 70 °C, 3 h at 150 °C and 2 h at 200 °C. Calcined powders were then obtained by calcination in air at 400 °C during 2 h with a rising step of 1 °C min^{-1}.

Prior to use, these substrates were ultrasonically cleaned in detergent, distilled water, acetone, ethanol and finally in distilled water for 15 min in each medium, then dried in air at 150 °C. For the spin-coating, the angular velocity range of the spinner was fixed at 2000 rpm. After the deposition of each layer, the coated slices were aged in air at room temperature for 12 h, and finally dried successively for: 6 h at 70 °C, 3 h at 150 °C and 2 h at 200 °C. This consolidation temperature was selected to finish the polycondensation step of the titania framework. Calcined films were then obtained by heating in air at 400 °C for 2 h with a temperature rise of 1 °C min^{-1}, which ensures complete removal of organic species (including the template, Supporting information), still avoiding cracks of the films. Choi et al. [17] show by TGA analysis that the degradation of the template (Pluronic P123) occurs between 120 °C and 280 °C, in fair agreement with our analysis. As reported by Nam et al. [19] this temperature is sufficient to obtain the anatase phase of TiO_2 film grown on SLG by sol–gel process. Finally, the samples were gradually cooled down to room temperature.

2.3. Films characterization

TEM analysis was performed using a LEO922 electron microscope operating at 200 keV. The film was scratched off from the substrate, dispersed in ethanol and then deposited on copper grids coated with a porous carbon film. The solvent was evaporated in air before the samples analysis.

Atomic force microscopy (AFM) imaging was performed in air at room temperature (~20 °C) using a commercial optical lever microscope (Nanoscope III, Digital Instruments, Santa Barbara, CA). Images were taken with a silicon nitride tip in tapping mode. Several scan were collected at different region of the sample to ensure that the shown images are representative.

Grazing incidence small-angle X-ray scattering was performed with a GISAXS-Rigaku S-max 3000 facility equipped with a micro-focus source $\lambda = 0.154$ nm and a 2D Gabriel type detector placed at 1494 mm from the sample. The incident angle was 0.2°. The transmitted and specular reflected beams were masked by a vertical beam-stop. Diffraction patterns were analyzed using Igor software.

X-ray photoelectron spectroscopy (XPS) was performed on a Kratos Axis Ultra spectrometer (Kratos Analytical, Manchester, U.K.). The residual pressure in the analysis chamber was lower than 10^{-6} Pa. The monochromatic Al X-ray source was powered at 15 kV and the emission current was 10 mA. The charge stabilization was achieved by using the Kratos Axis device. The analyzed area was 700 μm × 300 μm and the pass energy of the analyzer was set at 160 eV for the survey scan and 40 eV for the narrow scans. The binding energy (BE) values were referred to the C—(C, H) contribution of the C 1s peak fixed at 284.8 eV.

Atmospheric ellipsometric porosimetry (A-EP) measurements were performed with an equipment from Sopra (Model GES-5E, A-EP, Sopra, Paris, France) using the software package "WinElli2". The A-EP is the combination of spectral ellipsometry and adsorption porosimetry. The data were fitted in the range between 1.6 eV and 4.5 eV using a Cauchy-type material as model layer to determine the film optical constants. Refractive index values were given for a wavelength of 633 nm and the films thicknesses were obtained for each measurement step. For the environmental porosimetric measurements, the ellipsometer chamber was flushed with a variable humidity flow of 2.5 L of air/min. The humidity was adjusted using a mass flow controller and monitored using a relative humidity (RH) probe placed in the environmental chamber. The open porosity was measured from the change of the optical characteristics (n: refractive index, k: extinction coefficient) and the variation of the film thickness during the water–vapor adsorption/desorption. The pore size distribution (PSD) was determined from the isotherm exploited via the modified Kelvin equation [20].

2.4. Photocatalytic efficiency

The photocatalytic activity of the films was evaluated by following the concentration decay of the Rh6G dye under monochromatic light irradiation (365 ± 5 nm) from Hayashi LA-310 UV lamp, equipped with Oriel 74000 monochromator. The deposition of the Rh6G on the photocatalyst samples prior to the test was done by spin-coating 0.1 ml of an ethanolic solution of Rh6G (1 mmol l^{-1}) and drying in air under dark condition. After illumination, the titania films were fixed onto the sample holder of the UV–vis–NIR spectrophotometer from Varian (model Cary 5E) equipped with an integrating sphere. Spectra were recorded with background correction in the wavelength range 200–800 nm during 300 min.

3. Results and discussion

3.1. Structural, textural properties and surface composition

Titania films with variables textural properties were obtained by using two kinds of nonionic block copolymer with a different molecular weight as templating agents. Mesoporous films were compared to dense TiO_2 film obtained by a template-free sol–gel process. The titania films were grown on SLG by spin-coating at 2000 rpm and then dried before calcination at 400 °C as detailed above.

TEM images of the scraped titania films prepared by sol–gel and calcined at 400 °C are shown in Fig. 1. The TiO_2 film synthesized from a free-template sol is dense and do not show any mesopores. On the contrary, the titania films obtained using Brij56 (TiB) and Pluronic P123 (TiP) as structure molding agents exhibit mesopores more or less regularly ordered. The pore size is in the range from 9 to 11 nm for TiP and 5 to 7 for TiB. The pores are separated by walls about 2–4 nm in thickness for each film.

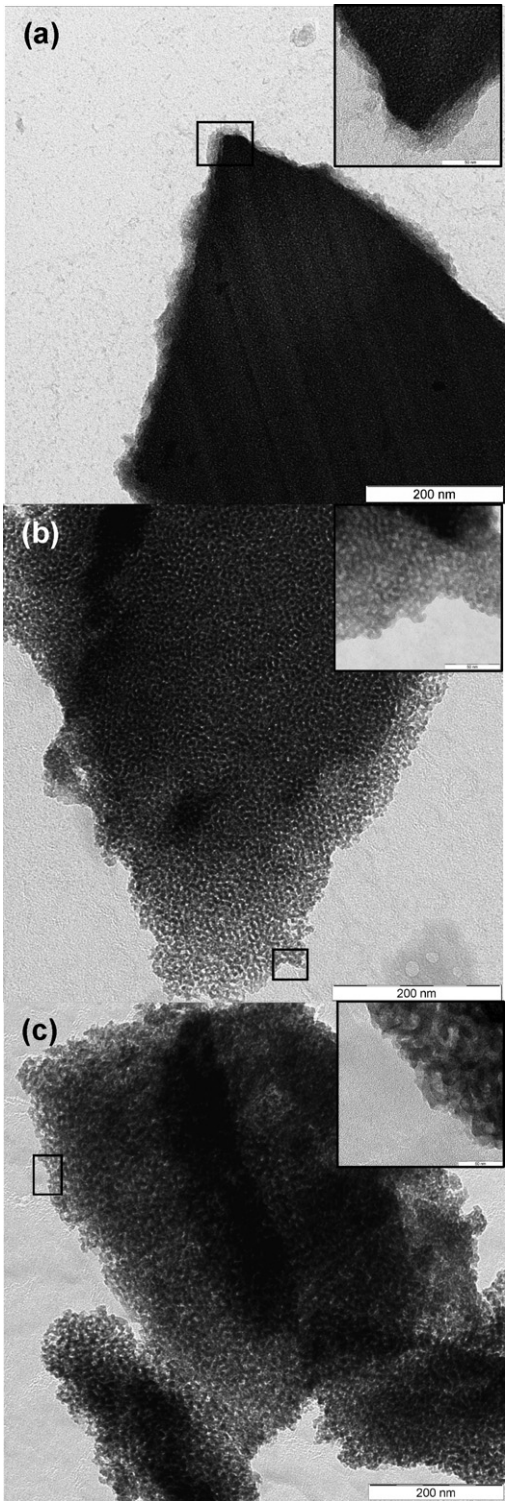

Fig. 1. TEM images of (a) template free TiO_2 and (b) mesoporous TiB and (c) TiP films obtained by sol–gel spin-coating process and calcined at 400 °C.

The surface topography of the films was analyzed by AFM. Fig. 2 shows a two-dimensional AFM image of the surface of titania films. The AFM images reveal a regular grain structure. The grain size for each film was estimated to be in the range from 5 to 10 for template-free TiO_2, 20 to 30 for TiB and 15 to 25 for TiP. The surface

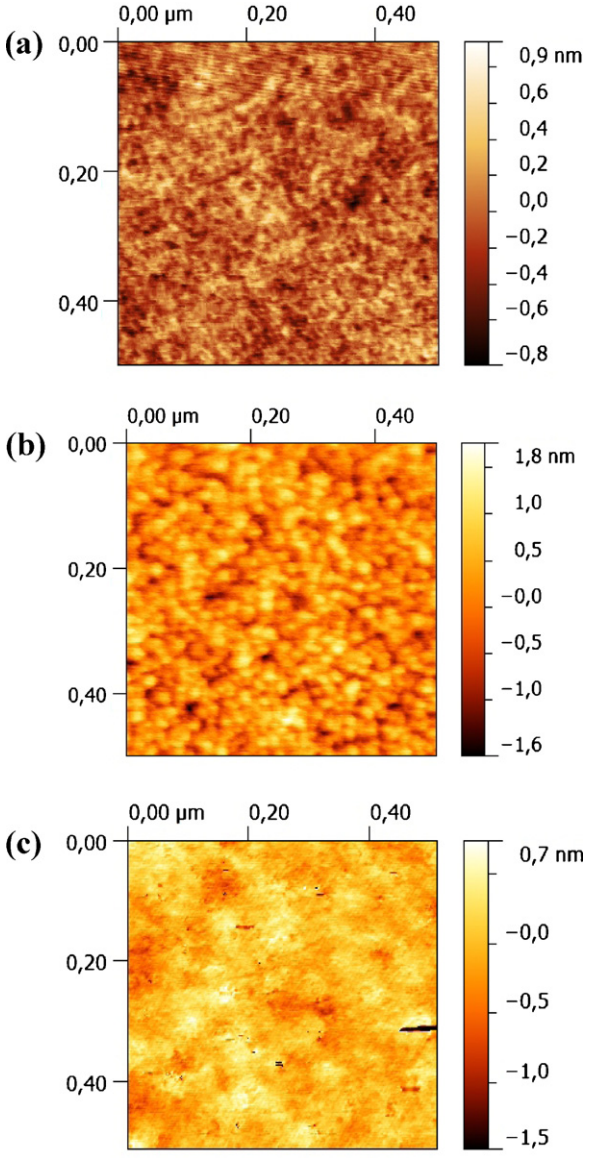

Fig. 2. AFM 2D images of the surface of (a) template-free TiO_2, (b) TiB and (c) TiP films.

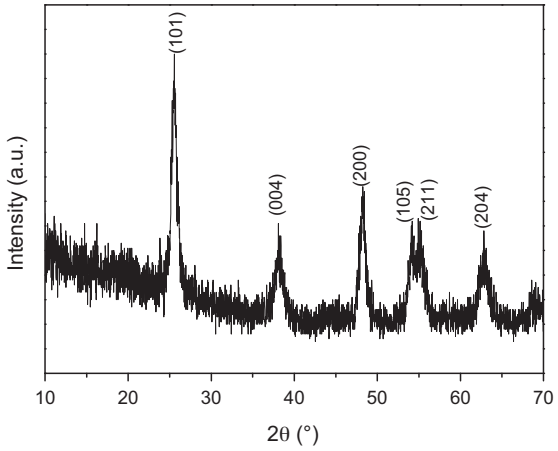

Fig. 3. X-ray diffraction pattern of the TiO_2 powder synthesized according to TiP procedure.

roughness of the films was obtained to be less than 1 nm for all films.

X-ray diffraction pattern of the powder prepared following the same procedure for that of the TiP film is shown in Fig. 3. The XRD pattern confirms that calcination at 400 °C led to the formation of crystalline TiO_2 with predominance of anatase phase (00-021-1272 JCPDS card number) with a preferential (1 0 1) orientation.

Fig. 4 shows the GISAXS patterns of the calcined films. They exhibit the characteristic pattern of organized mesoporous films for TiB and TiP. The rather wormlike pore structure seen in TEM is confirmed by GISAXS. The faint ellipsoidal circle corresponds to domains that have the same structure, but with random orientation with respect to the surface [21]. The rod-like spots seen on the 2D patterns indicate that the films are partly crystallized [22]. The GISAXS intensity profile diagrams (Fig. 4a′ and b′) are obtained after radial integration of the exposed image plates. The diffraction angles correspond to d-spacing of 7.3 and 11.8 nm respectively for TiB and TiP. The TiO_2 film, on the other hand is not structured at all (not shown).

The surface chemical composition of the titania films was investigated by X-ray photoelectron spectroscopy (XPS). The results for all samples are listed in Table 2. Fig. 5 shows high-resolution XPS spectra of all elements detected at the surface of TiP. An example of a general XPS spectrum of the surface of TiP thin film is also shown in Fig. 5a. The peaks characteristic of titanium, oxygen, carbon, chlorine and alkali metals can be observed. The spin–orbit components ($2p_{3/2}$ and $2p_{1/2}$) of the Ti 2p peak were well resolved by two curves centered at 458.2 and 463.9 eV (Fig. 5b). The separation between the Ti $2p_{3/2}$ and Ti $2p_{1/2}$ peaks is 5.7 eV, consistent with the presence of Ti^{4+} in a tetragonal structure characteristic of a crystalline TiO_2 thin film [23]. The O 1s region is composed of several peaks. The main peak at 529.8 eV is attributed to oxygen involved in Ti—O bonds in TiO_2. The other two oxygen peaks can be assigned to oxygen in the O—H bonds of the hydroxyl groups and in H_2O and C—O. A carbon C 1s peak was observed at 284.8 eV for all the samples. This peak is related to the residual carbon from titanium (IV) tetraethoxide precursor decomposition and some surface pollution due to the exposition of the samples to air before XPS analysis. The presence of alkali elements such as Na, K, and other elements such as Si, Ca and Mg in the XPS survey spectra (see Fig. 5e–g) indicates the occurrence of diffusion from the SLG substrate into the TiO_2 film during calcination. Chlorine is present as a residual compound from the acidic condition (HCl 37%) used during the sol synthesis.

Fig. 6a shows the adsorption/desorption isotherms of the template-free TiO_2, TiB and TiP films reconstructed from the ellipsometry data using the Bruggeman effective medium approximation (BEMA) model. The adsorption/desorption curves of water remain close to 0% for the template-free TiO_2, indicating the absence of open porosity. On the contrary, a reversible type IV-adsorption/desorption isotherm with an hysteresis loop was observed for the TiP film, indicating the presence of mesopores (according the IUPAC adsorption isotherm classification [24]). The adsorption curve reveals a marked step around RH = 60%, the steep evolution of which indicating the narrow distribution of the pore size. This means that when increasing RH the open mesoporosity is filled by condensed water. The adsorption isotherm for TiB film corresponds to a type V-adsorption/desorption, indicating a weaker interaction between the adsorbate and the adsorbent. The open porosity was estimated to be 28% and 44.3% (in volume) for TiB and TiP, respectively. The pores exhibit a cylindrical morphology since the square of the partial pressure at the condensation of the water into the pore volume was equal to the partial pressure at the decondensation during the desorption. The pores extremities are open and could be interconnected with each other. Fig. 6b displays the respective differential pore size distributions calculated

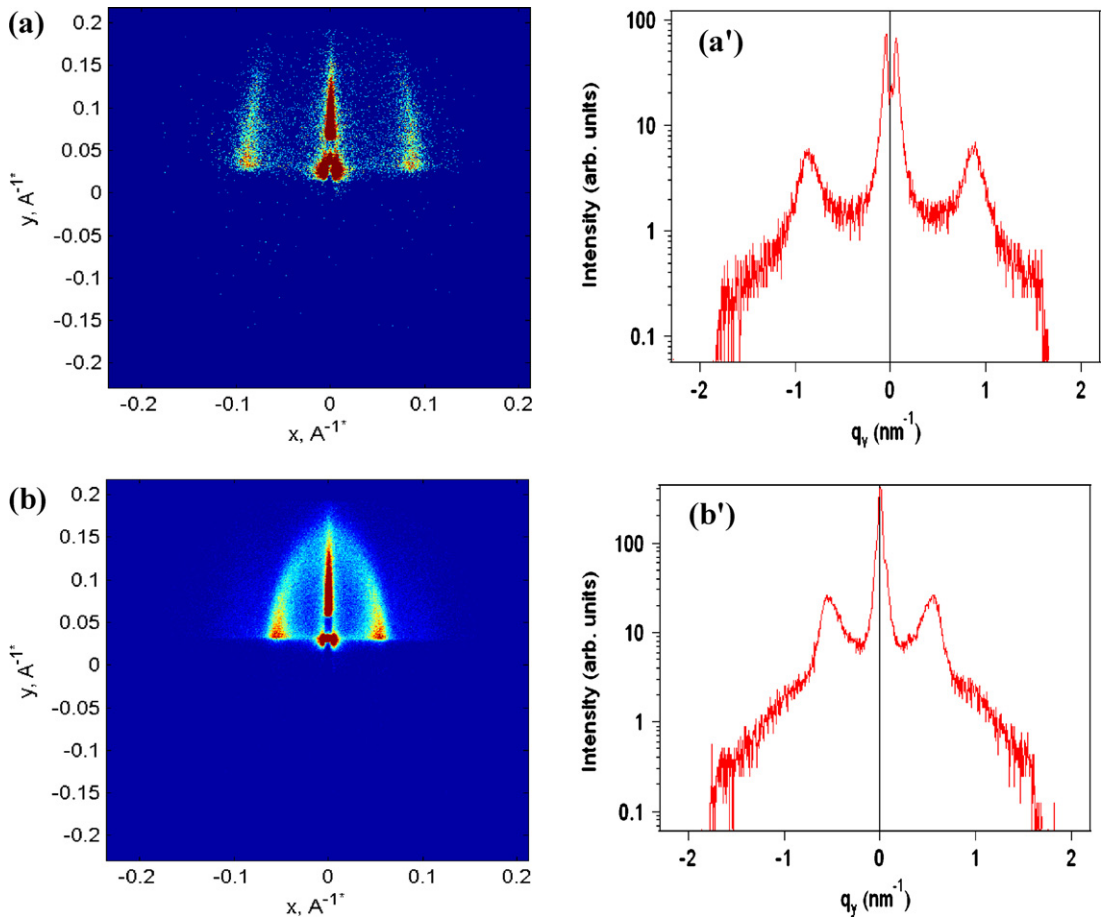

Fig. 4. (a and b) GISAXS patterns and (a′ and b′) GISAXS intensity profile of TiB and TiP calcined films, respectively.

Table 2
Surface composition content of titania films as determined by XPS expressed by at%.

Sample	O—Ti	Ti 2p	C—(C, H)	Cl 2p	Si 2p	K 2p	Ca 2p	Mg 2p	Na 1s
TiO_2	37.3	19.3	12.4	0.8	1.3	0.2	0.4	2.4	7.7
TiB	28.57	16.8	13.4	0.5	2	0.2	0.4	2.9	8.3
TiP	31.4	16.5	10.7	0.7	2.1	0.3	0.5	2.8	10.2

from the adsorption/desorption branches using the modified Kelvin equation and employing the respective water contact angle of the coatings measured after that the films were ultrasonicated under ethanol ($\theta \approx 10^\circ$). They revealed that pore diameters deduced from the adsorption curve were 8 and 14 nm for the TiB and TiP, respectively. These values are in fair agreement with the TEM estimation (see Table 3). The desorption curve indicates that the pores were connected by a narrow size distribution neck of which the size is about 5 and 5.6 nm respectively for TiB and TiP.

The refractive index of the films obtained at 633 nm in dry condition is reported in Table 3. The template free TiO_2 shows a refractive index of 2.18 close to that for a dip-coating deposited TiO_2 anatase film treated at 450 °C [8]. The mesoporous TiB and TiP films show a weaker value of refractive index (see Table 3). Obviously, the porosity increases the optical transparence of the titania films. In the case of the highly porous TiP, the refractive index ($n_{TiP} = 1.51$) is close to that of the SLG substrate. This results in an increase in film transmittance up at 460 nm. The porosity of the films can be calculated from the formula [25]

$$f_c = \left[1 - \frac{n^2 - 1}{n_\tau^2 - 1}\right] \times 100\% \quad (1)$$

where n is the refractive index of the film and n_τ is the refractive index of bulk TiO_2 ($n_\tau = 2.49$ for anatase [26]). The calculated values of porosity of the annealed films are given in Table 3. The calculated

Table 3
Optical and textural characteristics (spherical pore model) obtained by atmospheric ellipsoporosimetric porosimetry.

Sample name	Thickness (nm)	$f_{A\text{-}EP}$ (%)	f_c (%)	n	d_p (nm) (TEM)	d_p (nm) (adsorption)
TiO_2	70	–	28	2.18	–	–
TiB	117	28	63	1.70	5–7	8
TiP	185	44.3	75	1.51	9–11	14

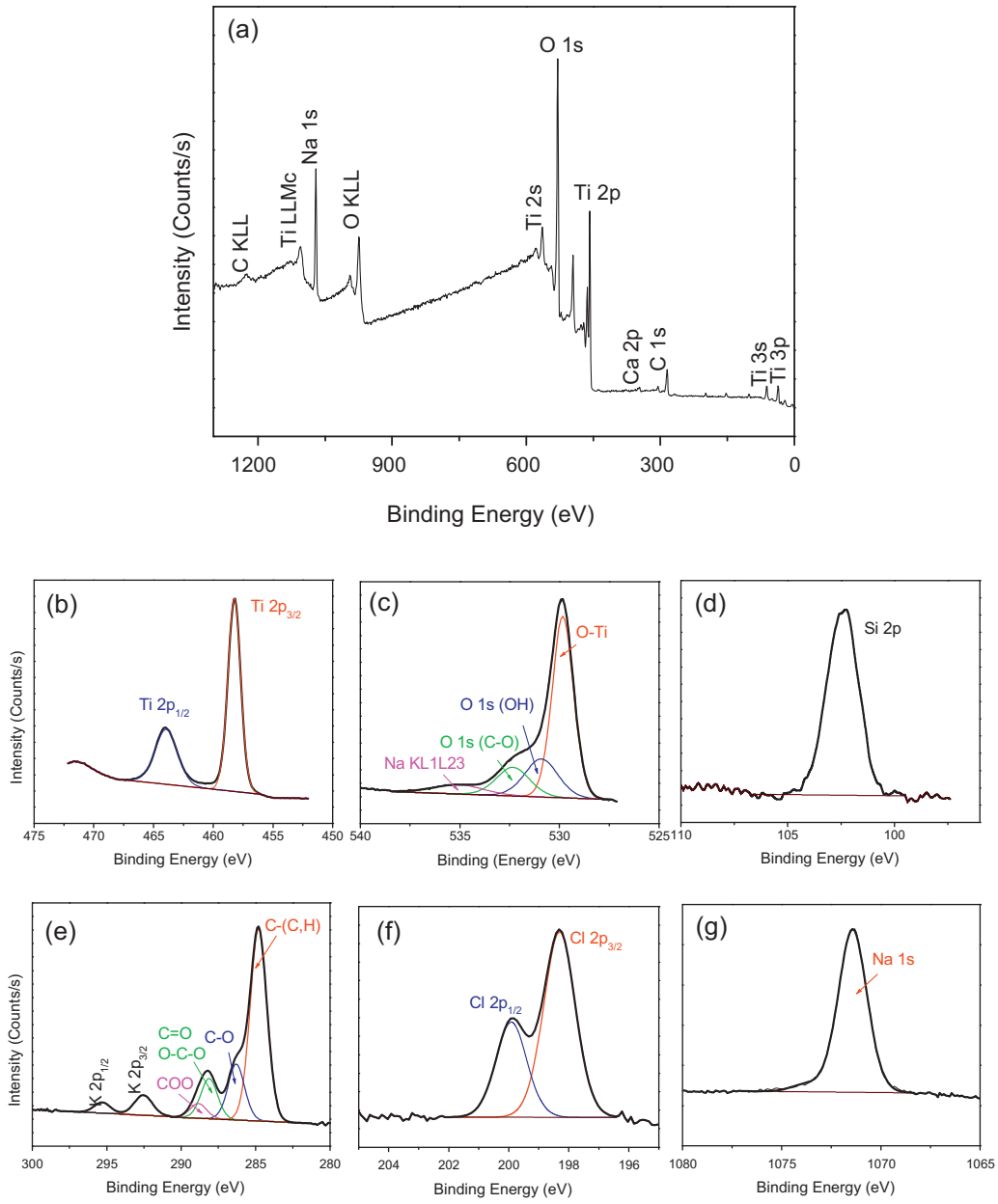

Fig. 5. XPS spectra of the surface of TiP film grown on SLG.

porosity (denoted f_c) was 30% superior to that obtained by A-EP. The difference can rationalize the lowest value of non-porous TiO_2 film compared to bulk TiO_2. Non-porous TiO_2 film prepared via sol–gel contained principally inaccessible porosity. This is in agreement with the fact that the A-EP measurement allows assessing only the accessible porosity (open porosity) during the water adsorption/desorption cycle, whereas the measure of the refractive index leads to quantify the *total* porosity of the titania films. Thus the fraction of closed pores can be estimated by difference. Fig. 7 shows the UV–visible spectra, ascertaining the transparency of the mesoporous TiP and TiB films by comparison to the template free TiO_2 film and SLG. The transmittance of titania mesoporous TiB and TiP films was about 92%, whereas that of the nonporous TiO_2 film was only 75–80%. The transmittance of the TiP grown on SLG was close to that of the naked SLG confirming that the high transmittance of the mesoporous films originates from their high porosity, low refractive index and high uniformity. These results are in accordance with the A-EP refractive index measurements.

3.2. *Aggregation form of Rh6G and photocatalytic activity*

The photocatalytic activity of the titania films was investigated under ambient conditions, through monitoring of the decay of the absorbance maximum of the Rh6G dye adsorbed on the films, as a function of the irradiation time. In our experiments, we used an ethanolic dye solution ($1\ mmol\ l^{-1}$) in order to reduce the tendency to form dimeric aggregates [27].

The adsorption spectra of Rh6G deposited on SLG, non porous and mesoporous titania films exhibit different features (Fig. 8). The spectra have maxima at approximately 530 nm, with a shoulder around 510 nm for the Rh6G adsorbed on mesoporous titania films. This shoulder is known to account for the H-form dimer, while the main absorption peak corresponds to the free Rh6G monomer [28]. A spectral red shift for both the peak and the shoulder (~20 nm) was observed in the case of the Rh6G adsorbed on template free TiO_2 and SLG. This bathochromic shift could be assigned to changes in the physicochemical properties of the

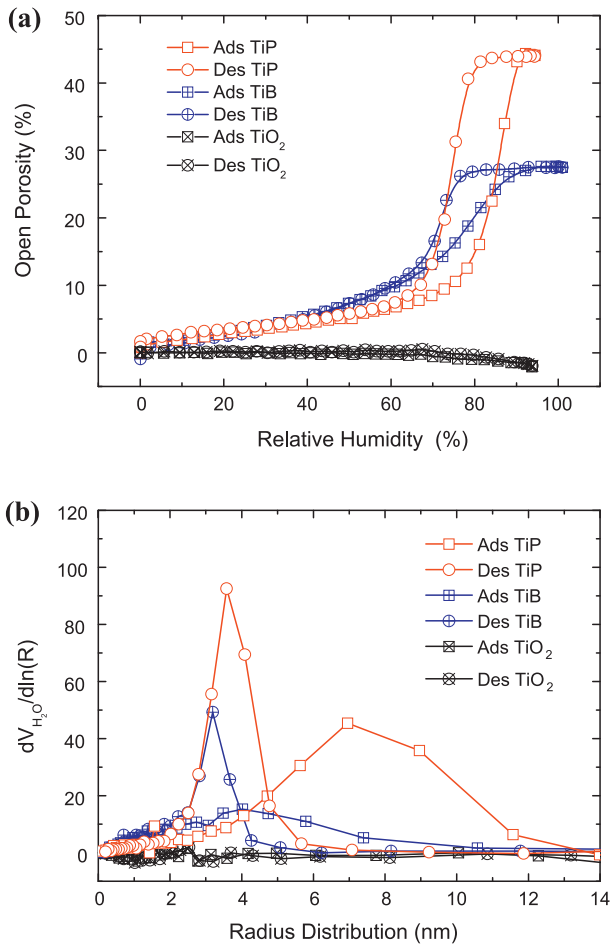

Fig. 6. Water adsorption/desorption isotherm of porous (TiB and TiP) and non porous (TiO_2-template free) titania films (a). Pore size distribution deduced from the adsorption and desorption branches of the titania films (b).

interlayer environment of the Rh6G [29]. The absorption band shape is also visibly affected by the nature of the film. Indeed, the relative absorbance of the shoulder (denoted A_{sh} for H-type dimers) with respect to the main absorbance (denoted A_{max} for free Rh6G monomers) band decreases with the pore fraction on the titania films. It is believed that this dependence is related to the surface texture of the titania films. This observation is illustrated by the decrease of the $R = A_{sh}/A_{max}$ with the increased film porosity into

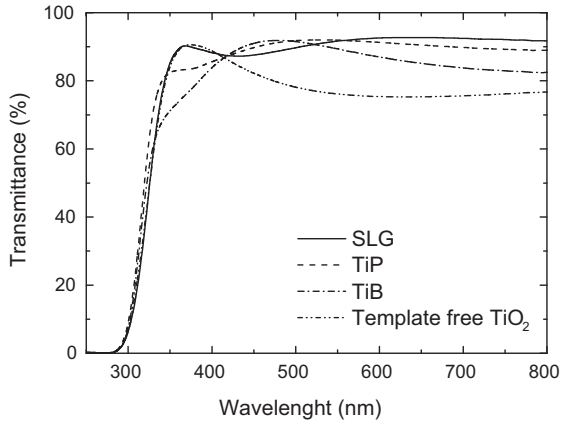

Fig. 7. UV–vis transmittance spectra of naked and coated SLG with different type of titania films.

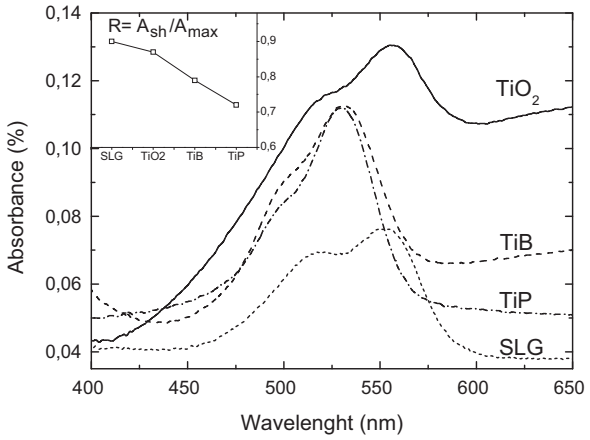

Fig. 8. UV–vis absorption spectra of Rhodamine 6G dye as soon as deposited on SLG and variable titania films.

the films (inset Fig. 8). This result shows that the porosity of the titania film affects the aggregation form of the adsorbed Rh6G. More than that, it seems that higher porosity favors a monomer dye adsorption at the surface. Similar observations were reported by Malfatti et al. [30]. The authors show that the aggregation form of the Rh6G was related to the initial concentration introduced into mesostructured silica films. At low concentration, the amount of the H-type dimeric aggregations was reduced and the formation of the fluorescent form at low wavelength was favored.

Rh6G was shown to be fairly stable under UV-irradiation but without photocatalyst (on naked SLG) allowing to consider direct photolysis as negligible (Fig. 9a). Fig. 9a and b shows the bleaching curves of each aggregation forms (monomer and dimer) of the Rh6G on the different samples. In the case of the monomer bleaching, the results show that the higher is the porosity into the titania films, the faster is the bleaching of the dye. As generally accepted in the literature, a highly porous surface structure is suitable because it offers a higher number of catalytic sites which in turns causes higher photocatalytic activity [10,11]. The evolution of Rh6G monomer concentration, as measured by UV–vis spectroscopy, as function of irradiation time for mesoporous films (TiP and TiB) follows a pseudo-first order, in agreement with the model described by Ollis [31] for porous films. Whatever the photocatalyst, it is observed that the degradation of the dimer form obeys a pseudo-zero order law. This situation suggests that the mechanism of the degradation of the Rh6G occurs in different ways for the two aggregation forms. The coexistence of the monomer and dimer forms on the photocatalyst surface induces probably a competition between them for photocatalytic sites and subsequently changes the apparent order of the reaction. In the case of the degradation of the dimers, it appears that the degradation rate is not related to the available surface area (Fig. 9b) since the most porous films shows the lowest activity. Nevertheless, the degradation of the monomer form was faster than dimers whatever the titania films. This suggests that the monomer is the first to be attacked. The photocatalytic degradation kinetic of the monomer was slowed by the degradation of the dimmers rendering the global reaction kinetic a pseudo-first order. At the early stages of the reaction, the ratio of each aggregation form should be taken into account to compare the efficiency of the photocatalyst films.

The degradation mechanism of the dye is of Langmuir–Hinshelwood (L–H) type and can be described by a pseudo-first order model when the dye concentration is low.

$$r = -\frac{dc}{dt} = k_a c \qquad (2)$$

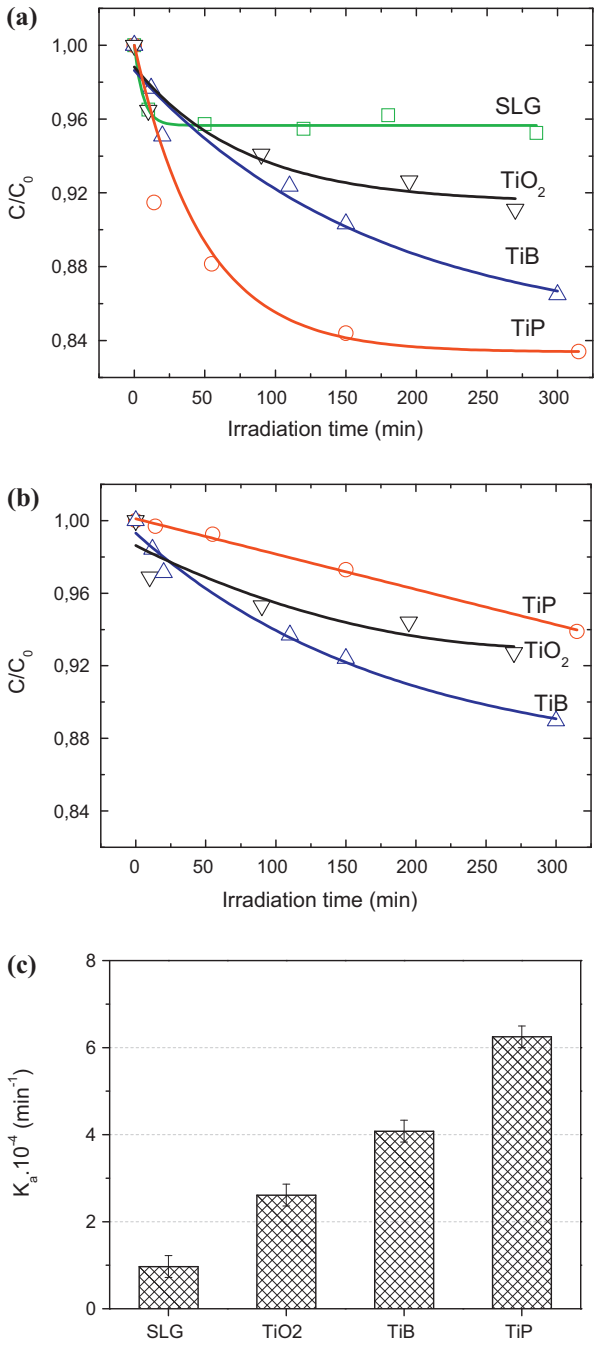

Fig. 9. Evolution of the normalized concentration of (a) monomer aggregation of and (b) dimer aggregation form of Rh6G dye for a naked SLG, templates free TiO_2, TiB and TiP films coated SLG as a function of irradiation time (c) and the corresponding bleaching rates (apparent kinetic constant k_a).

where r is the bleaching rate, t the irradiation time, c the dye concentration and k_a the apparent reaction rate.

According to the L–H mechanism, the degradation of the Rh6G occurs by means of a direct reaction with the photogenerated electrons/holes or by photocatalyzed oxidation via radicals ($OH^{\bullet}$) formation. The degradation via dye photosensitization can be excluded as the Rh6G was transparent at the wavelength (365 nm) used for the irradiation of the titania films. The reactant was randomly distributed at the photocatalyst surface and it takes a variable aggregation form, as assumed in our case. The kinetic of the reaction would result from a combination of the respective degradation rate due to the different degradation mechanism of each aggregation form. To compare the photocatalytic activity of variable titania films, we propose to evoke the contribution of each Rh6G aggregation form on the total apparent kinetic constant rate. Considering the proportion of the different aggregation forms of Rh6G, the degradation rate can be expressed as follows:

$$r_T = x\left(-\frac{dc_m}{dt}\right) + y\left(-\frac{dc_d}{dt}\right) \quad (3)$$

where r_T is the total bleaching rate, t the irradiation time, x and y are the proportion of the monomers and dimers of the dye and c_m and c_d are the concentration of monomers and dimers of Rh6G respectively.

The apparent rate constant is shown in Fig. 9c after the consideration of monomers and dimers aggregation forms of Rh6G with respect to their respective ratio on each titania films. The results show that the kinetic of the degradation of Rh6G follows the evolution of the porosity into the films. However, the available surface area alone does not explain the improvement of the photocatalytic activity but its contribution was indirect. During the spin-coating of the dye, the interaction between the TiO_2 film and the Rh6G molecules was probably influenced by the surface morphology. Then, the increase in surface area of the titanium film reduces the fraction of dimer and, consequently, increases the photocatalytic reaction, since the degradation of the monomer is faster.

4. Conclusion

Mesoporous titania films were obtained by addition of non ionic template in adequate concentrations in the starting sol. The films present a variable fraction of pores. TiB and TiP films present an ordered porosity which is randomly distributed onto the films. UV–visible spectroscopy showed that high available surface area of the titania films favors preferential formation of the aggregation of the Rh6G in a monomeric form. Furthermore, high porosity and surface area implicate higher contact surface to the Rh6G and then enhance the photocatalytic degradation rate. However, the photocatalytic performance do not only depends on the textural parameters of the titania photocatalyst but are also related to the aggregation form of the dye at the photocatalyst surface. The higher fraction of the monomer form in the porous film with larger pore size and porosity could be initiated by the higher adsorption capability in the pore channels. This makes easier the dye degradation and thus increases the disappearance rate of the dye at the photocatalyst surface.

Acknowledgments

M. Selmanne and C. Sanchez (Laboratoire de Chimie de la Matière Condensée de Paris) are gratefully acknowledged for providing access to the GI-SAXS facilities. Reasearcher from UCL are grateful to the "RégionWallonne" (Belgium) for his financial support. M.N.G. is grateful to R. Gigo for AFM measurements. D.P.D. thanks the FNRS for his post-doctoral researcher position.

Appendix A. Supplementary data

Supplementary data associated with this article can be found, in the online version, at doi:10.1016/j.apcatb.2011.12.016.

References

[1] A. Fujishima, K. Honda, Nature 238 (1972) 37–38.
[2] R. Wang, K. Hashimoto, A. Fujishima, M. Chikuni, E. Kojima, A. Kitamura, M. Shimohigoshi, T. Watanabe, Adv. Mater. 10 (1998) 135–138.
[3] A.I. Kontos, A.G. Kontos, D.S. Tsoukleris, G.D. Vlachos, P. Falaras, Thin Solid Films 515 (2007) 7370–7375.
[4] M.N. Ghazzal, N. Chaoui, M. Genet, E.M. Gaigneaux, D. Robert, Thin Solid Films 520 (2011) 1147–1154.

[5] A. Testino, I.R. Bellobono, V. Buscaglia, C. Canevali, M. D'Arienzo, S. Polizzi, R. Scotti, F. Morazzoni, J. Am. Chem. Soc. 129 (2007) 8566–8576.
[6] H. Cheng, J. Ma, Z. Zhao, L. Qi, Chem. Mater. 7 (1995) 663–671.
[7] C. Guillard, H. Lachheb, A. Houas, M. Ksibi, E. Elaloui, J.-M. Herrmann, J. Photochem. Photobiol. A: Chem. 158 (2003) 27–36.
[8] N.M. Ghazzal, N. Chaoui, E. Aubry, A. Koch, D. Robert, J. Photochem. Photobiol. A: Chem. 215 (2010) 11–16.
[9] B. Guo, Z. Liu, L. Hong, H. Jiang, J.Y. Lee, Thin Solid Films 479 (2005) 310–315.
[10] N. Arconada, A. Duran, S. Suarez, R. Portela, J.M. Coronado, B. Sanchez, Y. Castro, Appl. Catal. B: Environ. 86 (2009) 1–7.
[11] Y. Sakatani, D. Grosso, L. Nicole, C. Boissière, G.J. de, A.A. Soler-Illia, C. Sanchez, J. Mater. Chem. 16 (2006) 77–82.
[12] K. Murugan, T.N. Rao, A.S. Gandhi, B.S. Murty, Catal. Commun. 11 (2010) 518–521.
[13] A. Mills, M. Sheik, C. O'Rourke, M. McFarlane, Appl. Catal. B: Environ. 89 (2009) 189–195.
[14] J.C. Yu, J. Yu, H.Y. Tanga, L. Zhang, J. Mater. Chem. 12 (2002) 81–85.
[15] A. Mills, M. McFarlane, Catal. Today 129 (2007) 22–28.
[16] P. Chin, D.F. Ollis, Catal. Today 123 (2007) 177–188.
[17] S.Y. Choi, M. Mamak, N. Coombs, N. Chopra, G.A. Ozin, Adv. Funct. Mater. 14 (2004) 335–344.
[18] P.C.A. Alberius, K.L. Frindell, R.C. Hayward, E.J. Kramer, G.D. Stucky, B.F. Chmelka, Chem. Mater. 14 (2002) 3284–3329.
[19] H.J. Nam, T. Amemiya, M. Murabayashi, K. Itoh, J. Phys. Chem. B 108 (2004) 8254–8259.
[20] C. Boissiere, D. Grosso, S. Lepoutre, L. Nicole, A.B. Bruneau, C. Sanchez, Langmuir 21 (2005) 12362–12371.
[21] B. Smarsly, D. Grosso, T. Brezesinski, N. Pinna, C. Boissière, M. Antonietti, C. Sanchez, Chem. Mater. 16 (2004) 2948–2952.
[22] D. Grosso, G.J. de, A.A. Soler-Illia, E.L. Crepaldi, F. Cagnol, C. Sinturel, A. Bourgeois, A. Brunet-Bruneau, H. Amenitsch, P.A. Albouy, C. Sanchez, Chem. Mater. 15 (2003) 4562–4570.
[23] P. Babelona, A.S. Dequiedt, H. Mostéfa-Sba, S. Bourgeois, P. Sibillot, M. Sacilotti, Thin Solid Films 322 (1998) 63–67.
[24] K.S.W. Sing, D.H. Everett, R.A.W. Haul, L. Moscou, R.A. Pierotti, J. Rouquerol, T. Siemieniewska, Pure Appl. Chem. 57 (1985) 603–619.
[25] B.E. Yoldas, D.P. Partlow, Thin Solid Films 129 (1985) 1–14.
[26] L.S. Hsu, D. Luca, J. Optoelectron. Adv. Mater. 5 (2003) 841–847.
[27] K. Kemnit, K. Yoshibara, J. Phys. Chem. 95 (1991) 6095–6104.
[28] F.L. Arbeloa, V.M. Martınez, T.A. Lopez, T. Arbeloa, I.L. Arbeloa, J. Photochem. Photobiol. C: Photochem. Rev. 8 (2007) 85–108.
[29] S. Yariv, D. Ovadyahu, A. Nasser, U. Shuali, N. Lahav, Thermochim. Acta 207 (1992) 103–113.
[30] L. Malfatti, T. Kidchob, D. Aiello, R. Aiello, F. Testa, P. Innocenzi, J. Phys. Chem. C 112 (2008) 16225–16230.
[31] D. Ollis, Appl. Catal. B: Environ. 99 (2010) 478–484.